Hindawi
Advances in Materials Science and Engineering
Volume 2019, Article ID 4210762, 11 pages
https://doi.org/10.1155/2019/4210762

Research Article

Selective Laser Melting of Diamond-Containing or Postnitrided Materials Intended for Impact-Abrasive Conditions: Experimental and Analytical Study

Ramin Rahmani, Maksim Antonov, and Lauri Kollo

Tallinn University of Technology, Department of Mechanical and Industrial Engineering, Ehitajate Tee 5, Tallinn 19086, Estonia

Correspondence should be addressed to Ramin Rahmani; ramin.rahmaniahranjani@ttu.ee

Received 31 October 2018; Revised 17 May 2019; Accepted 15 June 2019; Published 26 June 2019

Academic Editor: Tomasz Trzepieciński

Materials with higher wear resistance are required in various applications including cutting elements (drag bits) of soft ground tunnel boring machines (TBM) to increase the productivity and to reduce the risk for workers involved in exchange operations (dangerous hyperbolic conditions). In recent work, two types of materials were produced by combining 3D printing (selective laser melting, SLM) of cellular lattice structures and spark plasma sintering (SPS) methods. The lattices were printed from (1) 316L stainless steel with diamond and (2) Ti6Al4V with nitriding. The effect of diamond content (5%, 10%, and 20%; nickel-coated particles) and unit cell size on performance was studied. The titanium alloy lattice was nitrided to increase its hardness and wear resistance. The effect of nitriding temperature (750°C, 900°C, and 1050°C) and lattice volume fraction (6%, 15%, and 24%, vol.) was investigated, and the optimized conditions were applied. The lattices were filled with 316L and Ti6Al4V powders, respectively, and consolidated by SPS. Samples were tested with the help of laboratory impact-abrasive tribodevice. Laboratory results have shown that both reinforcing approaches are beneficial and allow improvement of wear resistance in impact-abrasive conditions with great potential for TBM or similar applications. Modelling with the help of finite element method has shown that lattice structure enables reduction of peak local stresses in scratching and impact conditions.

1. Introduction

The combination of simultaneous production methods allows production of materials with improved properties. Materials with higher wear resistance are required in various applications including mining, cutting, drilling, and tunnel boring machines (TBM) to increase the productivity and to reduce the risk for employees and time required for exchange operations. Selective laser melting (SLM) and electron beam melting (EBM) are becoming the most popular techniques in additive manufacturing technology that are developed quickly during the recent decade. Very popular directions are solid prototype complex parts, porous electrothermal and acoustic materials, and lightweight metallic cellular lattice structures. The possibility to create structures with varied lattice cell size, volume fraction, layer thickness, and strut diameter from various metallic alloys has been very useful for the needs of biomedical, dental, and aerospace industries [1–3]. Starting from the invention of the SLM method, the most researched materials from the groups of stainless steel, titanium, and aluminium alloys were 316L [4], Ti6Al4V [5], and ALSi10Mg [6] due to their rounded shape of powders, good fluidity, great number of suitable applications, and high mechanical properties. Not many studies have been reported regarding other alloyed metals or composite materials. For example, 3D printing of diamond particles (as the hardest material with super hard crystals) needs extremely high temperature, pressure, and laser current. Since it is not possible with current 3D printers, designing special printers or mixing diamond particles with other powders is inevitable. Hence, a combination of lattice 3D

printing and additional postprocessing steps to improve lattice or to consolidate material allows achievement of improved properties required for wear resistance applications. Overall, SLM technique like all other technologies has advantages and drawbacks, such as using the same computer-aided design (CAD) model for printing, manufacturing of fully dense solid or porous parts, printing of complicated parts (implants, for example), ability of simultaneous duplication of the object with the same or various scales and required number versus high cost of powders and apparatuses, part dimension restrictions (to fit into volume of printer's chamber), long process duration for large parts, and required removal and postpolishing operations.

The gyroid periodic lattice structures manufacturability and influence of different unit cell sizes have been studied, and it was found that cell with size being as small as 2 mm can be built without supporting structures (self-supported) [7]. It is usually used to create the first level (*support*) of 3D printed materials adhering to the base platform. Then, there is commonly one solid layer (about 0.1 mm thick that corresponds to about four layers of 25 μm each) between support and following lattice structure to connect them that is called *spacer*. Finite element modelling of body-centred cubic (BCC) structure and the same one with a vertical pillar (BCC-Z) was discussed and compared with experimental samples to illustrate stress and stiffness under loading [8]. Support is helping to fix the printed structure to the platform without causing thermal stress-induced distortions. The effect of support dimensions, volume fraction, and unit cell size of lattice has been compared for gyroid and diamond lattice structure types [9]. Advanced gyroid-type 316L lightweight stainless steel lattice structures with a wide range of volume fractions, unit cell sizes, and orientations have been designed to avoid wastage of material powders to assure an acceptable coincidence of 3D printed and original CAD models [10]. The comparison between SLM-manufactured parts and a CAD model of self-supported diamond-type AlSi10Mg structures has been investigated, and good geometrical compliance and precise mechanical property prediction were demonstrated; however, lattice strut and pore size were slightly higher and lesser than the designed model, respectively [11]. An optimized Ti6Al4V open-cell lattice has been reported along with strain energy calculations, and strength to weight and stiffness to weight ratios [12].

Many of the recent articles more frequently have focused on the adaptation of analytical (finite element model or CAD design) and experimental (SLM manufacturing) results regarding the influence of strut size, cell size, support necessity, and optimum lattice type. Effect of laser power and scanning speed on strut diameter has been thoroughly investigated, and it is in direct proportion with laser power if constant scanning speed is used [13]. The study of AlSi10Mg gyroid-type cellular lattices has confirmed that an increase in the volume fraction of lattice material leads to rising of compressive strength while the increase in unit cell size leads to lower microhardness [14]. It was also found that build orientation of layered manufacturing and heat treatment condition of Ti6Al4V diamond-type cellular lattices under high pressure of hot isostatic pressing (HIP) is of high importance [15]. Meanwhile, spark plasma sintering as the pulsed electric current method produces near theoretical densified and fast consolidated samples in comparison with conventional powder metallurgy methods. Passing electric current through graphite die has the potential of sintering ceramic-metal mixed powders in nanostructure scale.

Two types of materials were produced by combining 3D printing (SLM) of cellular lattice structures and spark plasma sintering (SPS) techniques (by adding diamond particles or by nitriding). Additionally, the effect of diamond particles content and unit cell size was evaluated to optimize materials for applications where resistance against impact-abrasive action is important (tunnelling, mining, geothermal drilling, etc.). The use of additive manufacturing in industrial applications can facilitate (enable) welding or fixation by bolting of new wear-resistant materials and production of lighter materials or components as it was demonstrated by the current work. The experimental data have supported the results of modelling (scratching and impacting) with the help of finite element (SOLIDWORKS/ANSYS) software. Shortage of finite element modelling of composites (lattice and hard material compact) produced by multistep processes (3D printing and powder metallurgy) under combined tribological loading (impact and abrasive) to assess machine components performance (buttons, inserts, drag bits, etc.) was the motivation of adding dynamic simulation (instead of static) in the current work.

2. Materials and Methods

Stainless steel grade AISI 316L is an austenitic iron-based (with chromium, nickel, and molybdenum additions), low carbon, and the nonmagnetic alloy used for corrosion resistance and additive manufacturing applications. The powders of 316L are spherical and have good flowability that is important for feeding of 3D metal printing machine. Powder (see Figure 1(a)) was supplied by Sandvik Osprey Ltd [16].

Ti6Al4V has excellent strength to weight ratio and a great potential for aerospace, biomedical, and surgical applications. Spherical Ti6Al4V powders (see Figure 1(b)) containing titanium, aluminium, and vanadium were supplied by TLS Technik GmbH [17].

Diamond-type cellular lattices have been printed by Realizer SLM50 machine from 316L and Ti6Al4V (Figures 2 and 3), respectively. The lattice structure was printed with the following parameters: the thickness of one printed layer: 25 μm, laser current: 3000 mA, exposure time: 600 μs, point distance: 1 μm, diameter: 20 mm, and height: 15 mm. Two new types of reinforcement approaches were investigated. The first type of materials was made of 316L stainless steel with a varied percentage of nickel-coated diamond particles. The reinforcement of the second materials was achieved by nitriding of Ti6Al4V lattice printed with different cell sizes. Six samples including two reference materials (316L and Ti6Al4V) with a description of SPS conditions are shown in Table 1. Reference samples (Nos. 5 and 6) are produced directly in the SPS without lattice structure inside. Spark

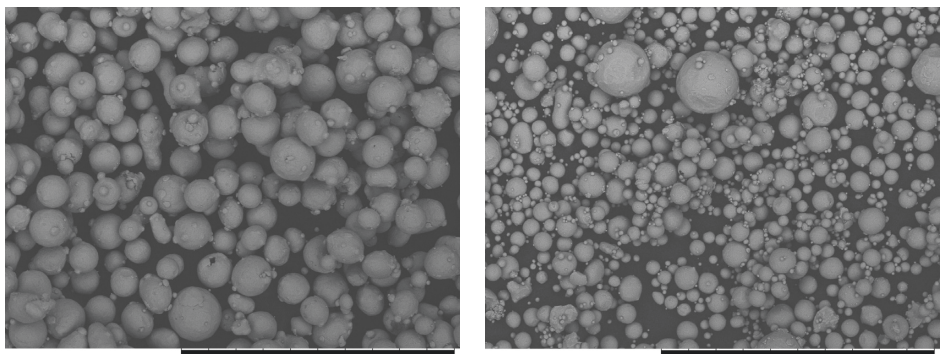

Figure 1: SEM micrographs of 316L and Ti6Al4V powders.

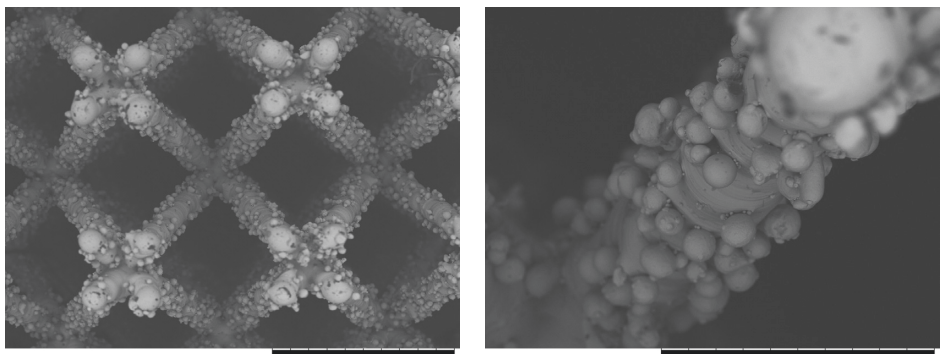

Figure 2: SEM micrographs of 3D printed 316L lattice.

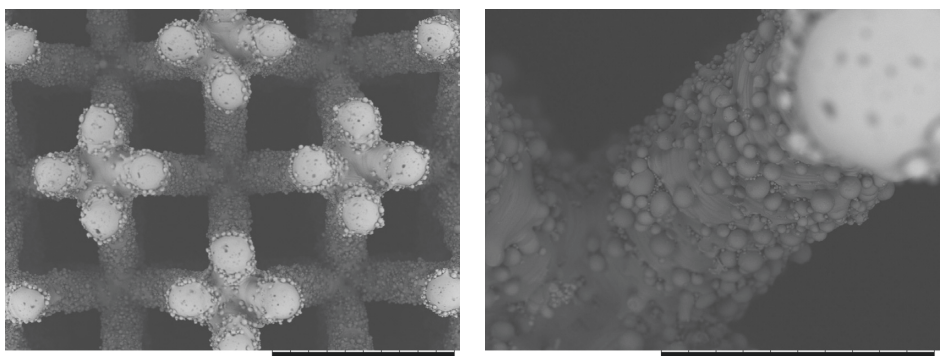

Figure 3: SEM micrographs of 3D printed Ti6Al4V lattice.

plasma sintering machine made by FCT Systeme, GmbH, was used for sintering of samples. Vacuum-nitriding furnace (VNF) made by R. D. WEBB, Ltd., was applied for nitriding of Ti6Al4V lattices at different temperatures.

In order to illustrate conditions in which the materials will perform (impact-abrasion), the cutterhead, drag bits, inserts, and buttons of TBM are schematically shown (CAD design) in Figure 4 according to [19, 20]. Additionally, the insert prepared by traditional powder metallurgy methods and 3D-printed structure ready for filling and the following consolidation by HIP or SPS are given in Figures 5(a)–5(c), respectively.

The first approach of reinforcement was realized by adding diamond particles into AISI 316L metal matrix prior to 3D printing of lattice. Diamond particles were covered by nickel coating (56 wt.%) to reduce diamond transformation

Table 1: Description of samples and SPS conditions.

Sample	Printed lattice	Filling powder	SPS conditions: temperature, pressure, sintering time
No. 1	316L-5%wt. diamond	316L	900°C, 75 MPa, 14 min
No. 2	316L-10%wt. diamond	316L	900°C, 75 MPa, 14 min
No. 3	TiN, 1.00 mm unit cell	Ti6Al4V	900°C, 75 MPa, 14 min
No. 4	TiN, 0.75 mm unit cell	Ti6Al4V	900°C, 75 MPa, 14 min
No. 5*	Without lattice	316L	1000°C, 50 MPa, 10 min
No. 6*	Without lattice	Ti6Al4V	1000°C, 50 MPa, 10 min

*5 and 6 are reference samples.

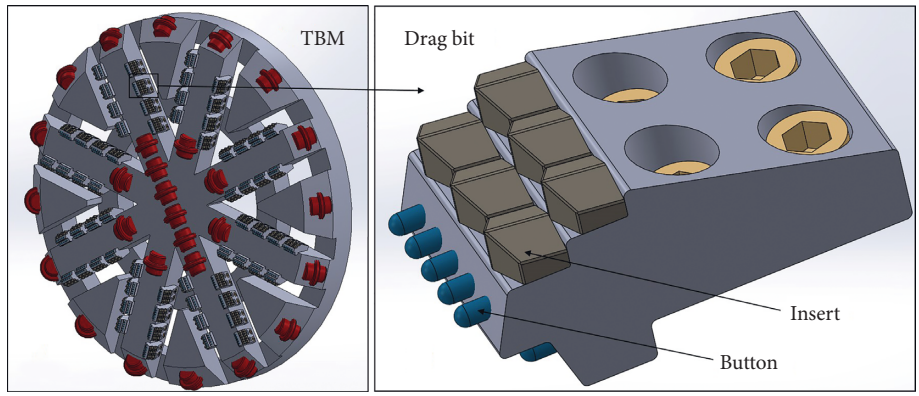

Figure 4: Schematic illustration of tunnel boring machine cutterhead (a), position of buttons and inserts in the drag bit (b) (TBM diameter is 3000 mm and drag bit dimension is 195 × 115 × 90 mm).

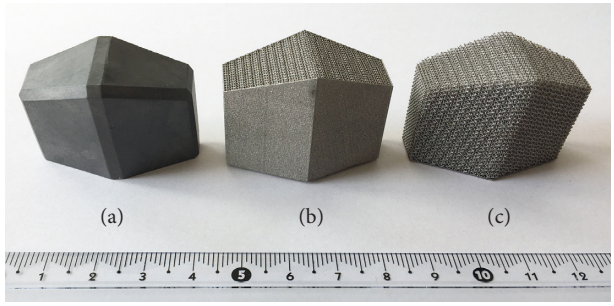

Figure 5: Tunnel boring machine insert produced by conventional powder metallurgy method (a), 3D printed structure for HIP (b), 3D printed structure ready for filling and following consolidation by SPS (c) (length, width and height of sample is 36 × 16 × 30 mm).

into graphite during 3D printing and sintering. Powder with 40–50 μm particle sizes was supplied by Vanmoppes & Sons Ltd. [18]. Stainless steel AISI 316L powder with 45 ± 10 μm particle size was obtained from Sandvik Osprey Ltd. Printed lattices with varied content of diamond in the 316L matrix are shown in Figures 6(a)–6(f). Comparison of structures with 5%, 10%, and 20% of coated diamond in Figure 6 displays that increase of diamond content leads in general to higher strut diameter and lower strength of lattice structure. On the other hand, the comparison between Figures 2 (plain AISI 316L) and 6 (AISI 316L with diamond) demonstrates that sticking of unmelted original metallic particles is reduced in case of printing with higher diamond content.

The second reinforcement approach is based on the creation of a hard titanium nitride phase (layer) by nitriding of titanium alloy lattice. Such reinforcement can provide improvement in wear and corrosion resistance of materials under study. Argon-atomized Ti6Al4V Grade 5 powders with ≤45 μm diameter and 4.429 gr/cm^3 density were used to print lattice structures with 30 l/h argon consumption, 25 μm layer thickness, 2 mm unit cell size, and 6% volume fraction of the material. In the second step, the Ti6Al4V lattice was heated in VNF under nitrogen gas flowing with 10°C/min heating rate and 90 min holding time at the desired nitriding temperature. Digital optical photos and SEM photographs of Ti6Al4V lattice structures with 2 mm unit cell size and constant nitrogen flow and different nitriding temperatures (750°C, 900°C, and 1050°C) are shown in Figures 7 and 8, respectively. No defects (like cracks) were detected after nitriding (Figure 8). It was found that nitriding at 900°C gives sufficient thickness of the nitrided surface layer and this temperature was selected as optimal. Additionally, Ti6Al4V lattices nitrided at 900°C temperature with varied volume fractions are shown in Figure 9. After printing and nitriding, the lattice was fulfilled with Ti6Al4V powders, sintered in SPS device. Plain (unreinforced) solid Ti6Al4V reference samples were directly sintered from raw powder. Comparison between Figures 3 and 8 (before and after nitriding) shows that there are no significant changes in lattice appearance. Unmelted attached particles are also nitrided and can serve as reinforcement.

3. Results and Discussion

3.1. Results of Laboratory Testing. Two types of reinforcement approaches were proposed for improving wear

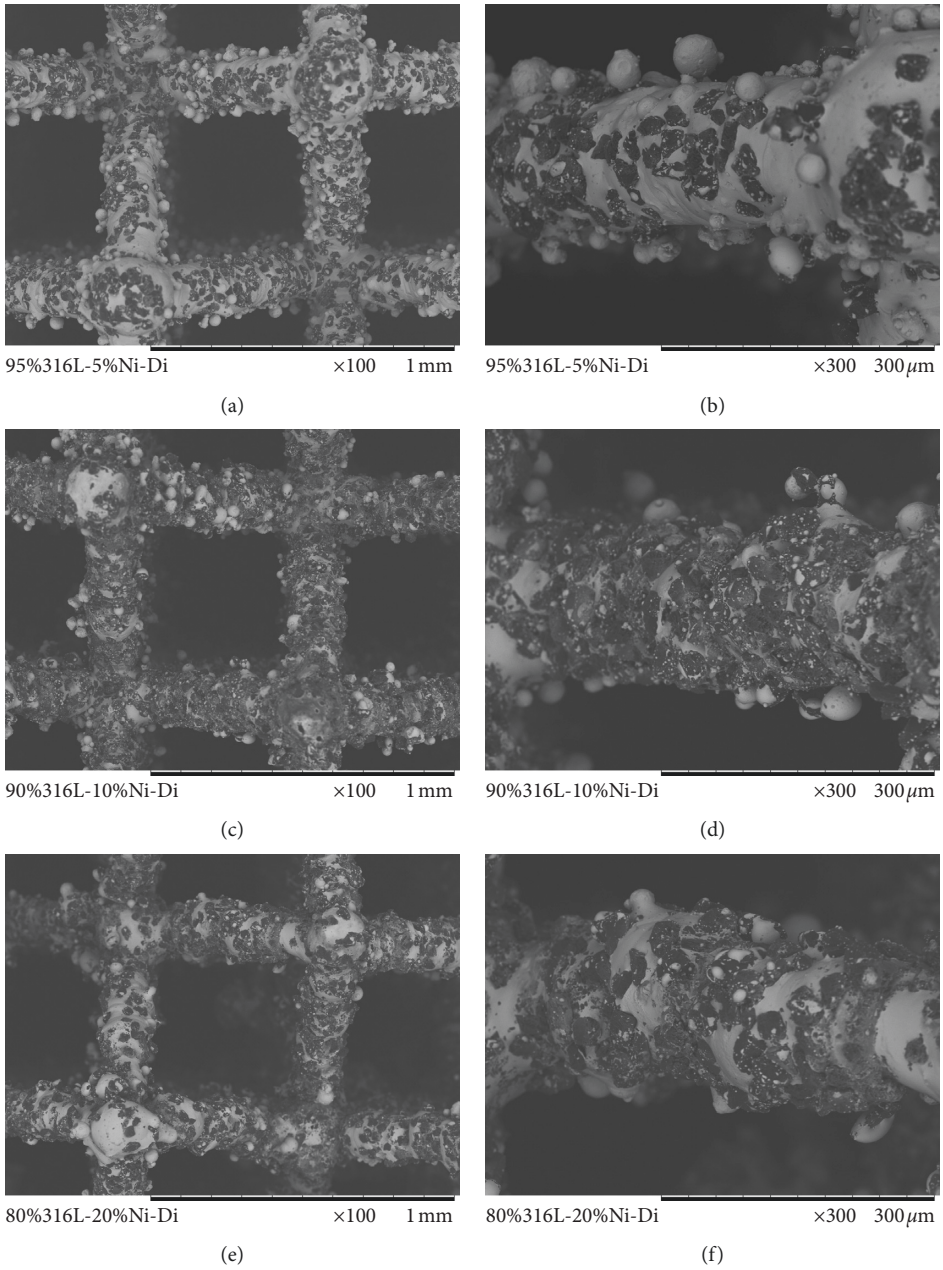

Figure 6: SEM images of 316L-diamond (nickel-coated) lattice.

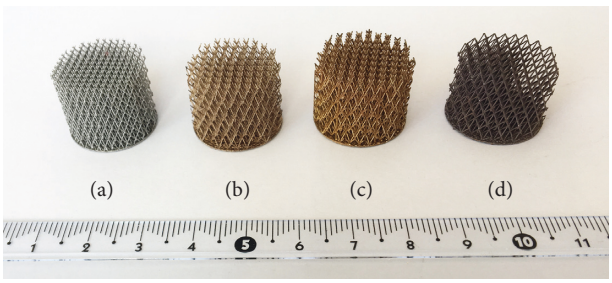

Figure 7: Digital photos of manufactured Ti6Al4V lattice (a) and heated and nitrided Ti6Al4V lattices at 750°C (b), 900°C (c), and 1050°C (d). Volume fraction and unit cell size are 6% and 2 mm, respectively (diameter of lattice structures is 20 mm, and length is 15 mm).

resistance and damage tolerance, namely, by diamond addition or nitriding. Possible arbitrary and/or uniform distribution of diamond particles in the metallic lattice and sample (Figure 6), finding the optimum condition for nitriding of Ti6Al4V lattice (Figure 7) and the effect of nitriding on microstructure of different metallic cell configurations (Figures 8 and 9), was introduced as novelty of recent research meant to improve wear resistance. After that, lattices were fulfilled by anticorrosive and ductile metals and sintered. Consequently, four samples have been prepared with the help of a combination of SLM and SPS techniques, and they are stated in Table 1.

Wear resistance of samples was evaluated via a custom-made patented impact-abrasive tribodevice (IATD) in

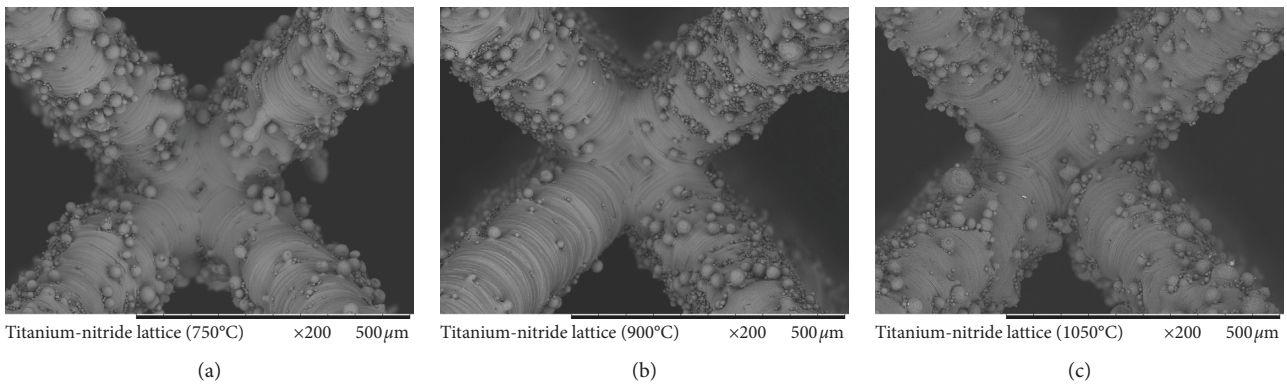

Figure 8: SEM images of Ti6Al4V lattices nitrided at various temperatures. Volume fraction and unit cell size are 15% and 1 mm, respectively.

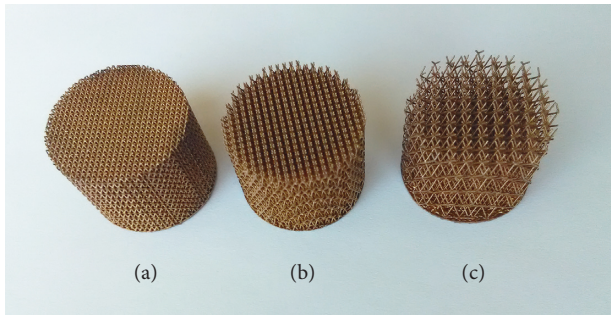

Figure 9: Digital optical photos of heated and nitrided Ti6Al4V lattices at 900°C with volume fraction and unit cell size of 26% and 0.75 mm (a); 16% and 1.00 mm (b); and 6% and 2.00 mm (c), respectively (diameter of lattice structures is 20 mm, and length is 15 mm).

Tallinn University of Technology [21]. Eventually, lost volume and a maximum depth of wear scar were evaluated by a *Brucker* optical surface profiler (OSP) ContourGT-K0+. Optical photographs of Sample No. 2 (as for example) after OSP assessment and also contour/perspective micrographs can be observed in Figure 10. Statistical results of lost volume as indicators of wear resistance of produced and tested materials are shown in Figure 11. The increase of coated diamond content improves the wear resistance of AISI 316L (compare Sample Nos. 1, 2, and 5). Hence, Sample No. 2 has better impact-abrasive behaviour than No. 1, and both of them are better than No. 5 (pure 316L without lattice as a benchmark). Combination of selective laser melting and spark plasma sintering has been introduced as a new approach for producing wear resistance material [22]. Hard material (diamond) coated by binder metal (nickel) filled inside cellular lattice structure (Ti6Al4V) showed anti-impact behaviour. Also, comparison between Sample Nos. 3, 4, and 6 shows that the nitriding enables improvement of wear resistance and a decrease of unit cell size (an increase of volume fraction) of Ti6Al4V-nitride lattice structure leads to higher wear resistance.

Postprocessing (nitriding or carburizing) can provide the increase in the Vickers hardness of metallic lattice structures up to 3 times [23]. Surface patterns of solid metallic structures have a significant role in controlling the friction coefficient [24]. Therefore, a cross section of rods in both lattice structure and surface of solid structures are important in tribology. Maximum depth of wear scar of Sample No. 2 (best result obtained by the addition of coated diamond particles) demonstrated in Figure 10 was 191 μm. Such good result was obtained by applying optimal SPS conditions enabling minimization of graphitization of diamond particles in a lattice structure that can protect the matrix against abrasion. XRD pattern of sample No. 4 (best result for Ti6Al4V-nitrided lattices structure) is depictured in Figure 12, illustrating that titanium nitride is formed and can provide protection against wear.

3.2. Results of Finite Element Analysis. Two finite element models for demonstration of the benefits of the lattice-included structure of TBM machine wear-resistant components (Figure 4(b)) are simulated by SOLIDWORKS and ANSYS software. TBM drag bit insert's abrasion (scratching or sliding) (Figures 13–15) and the impact of a button (Figures 16–18) were considered. The wear resistance of the plain sample, lattice structure, and contact with abrasive particle has been modelled by finite element simulation [25]. The results show the ability of lattice to absorb energy and decrease the rising of local stresses. Solid diamond (without lattice) and diamond with Ti6Al4V lattice were compared in both cases. The first simulation includes sliding of TBM insert against the wall (steel) designed in SOLIDWORKS and is demonstrated in Figure 13(a). The steel material (as counterpart) was chosen to illustrate the behaviour in most critical conditions. The meshing of the components and defining of boundary conditions were done with the help of ANSYS workbench analyser and AUTODYN solver as it can be seen in Figure 13(b). Strut diameter of modelled lattice structure was 200 μm, and unit cell size was $1 \times 1 \times 1$ mm. Sliding speed was set as 1 m/s, and distance was 1 m. Deformation and Von Mises stress distribution of pure diamond at the end of abrasion are demonstrated in Figure 14. It is possible to see that the stress exceeds that of compressive strength of diamond and pure diamond is broken in several locations while a diamond with lattice (Figure 15) experiences mainly minor deformation with some loss of extruded

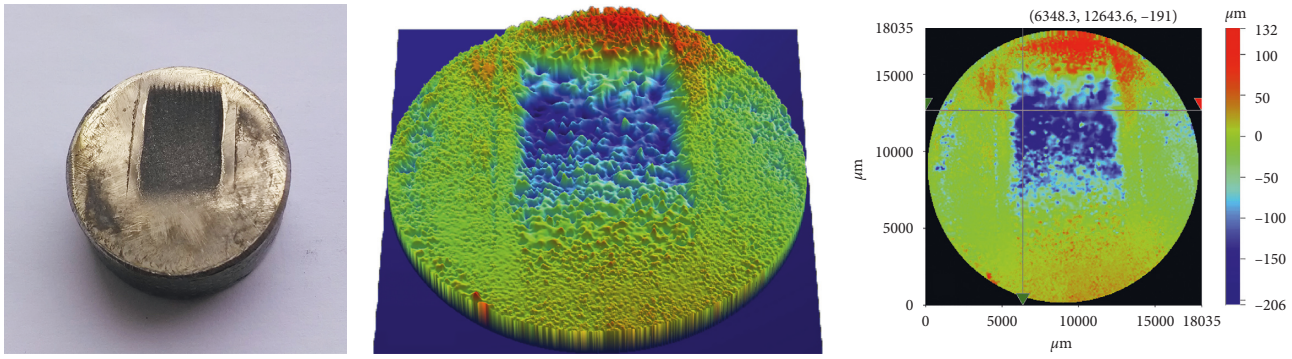

(a) (b) (c)

Figure 10: Optical image of Sample No. 2 after IATD test (a); OSP perspective micrograph (b); OSP height map micrograph (c).

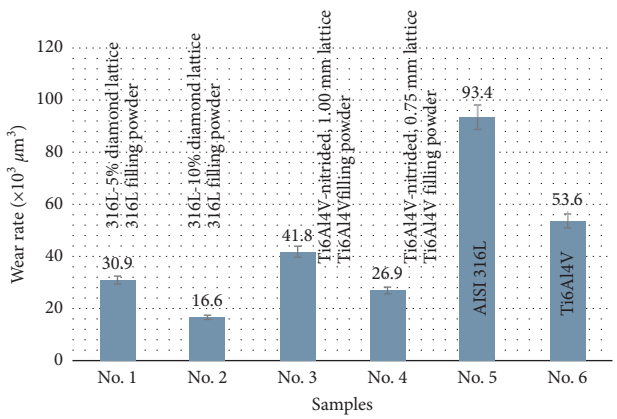

Figure 11: Wear rates of materials during impact-abrasive test.

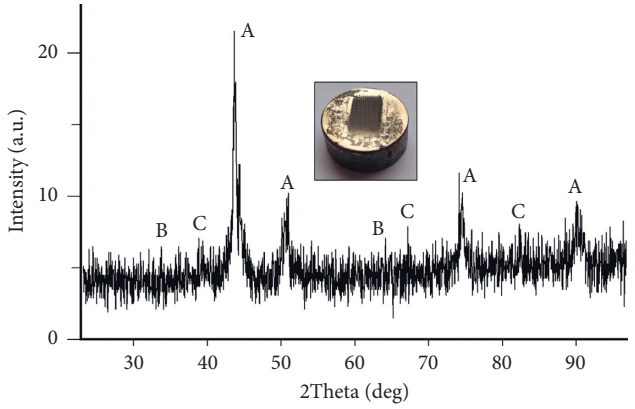

A: TiN
B: Ni_2V
C: $TiNi_2Al$

Figure 12: XRD pattern of Sample No. 4 (as example).

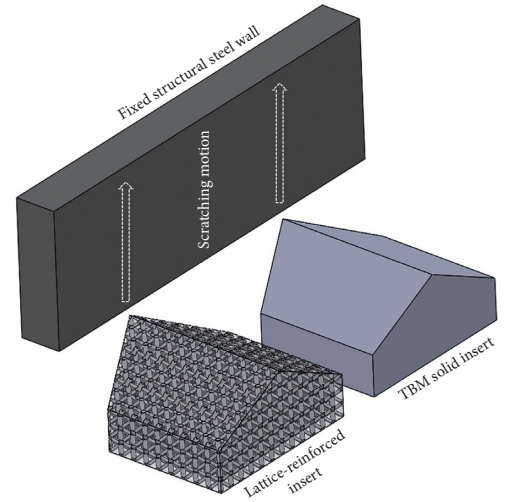

(a)

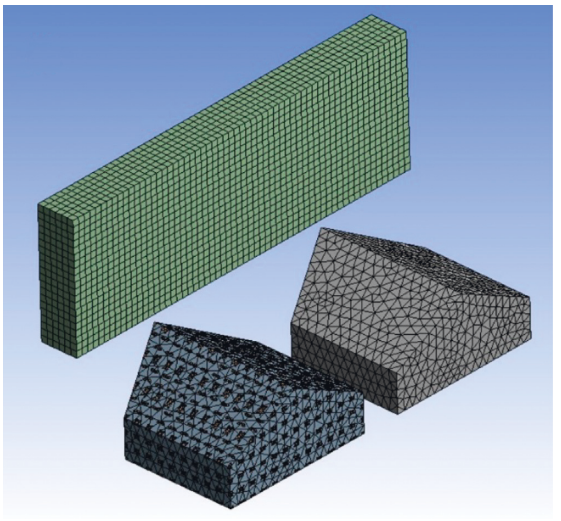

(b)

Figure 13: SOLIDWORKS design of solid diamond and diamond with lattice inserts (a); ANSYS mesh of solid and lattice-containing inserts (b).

metal lattice (diamond fragments were not lost). The area of the heavily affected zone of the insert with lattice structure is smaller (Figure 15(c)).

The second simulation was performed to analyse the process of the dynamic interaction of single TBM drag bit button with big stone to show the performance of material containing lattice against impact (Figure 16). The inertia of the button (inertia of cutterhead) and that of the stone were added to bring the conditions of modelling as close as

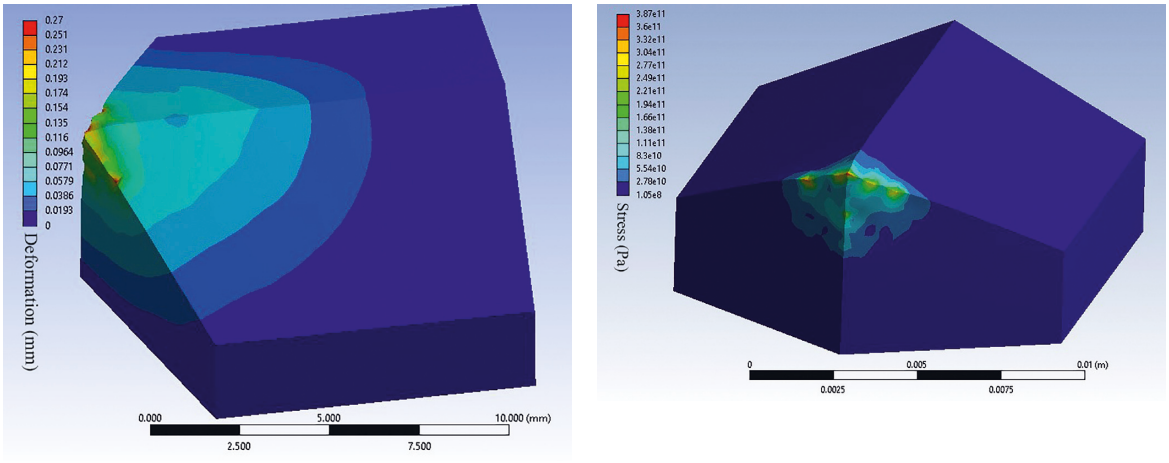

(a) (b)

Figure 14: Deformation (a) and Von Mises stress distribution (b) of solid diamond insert.

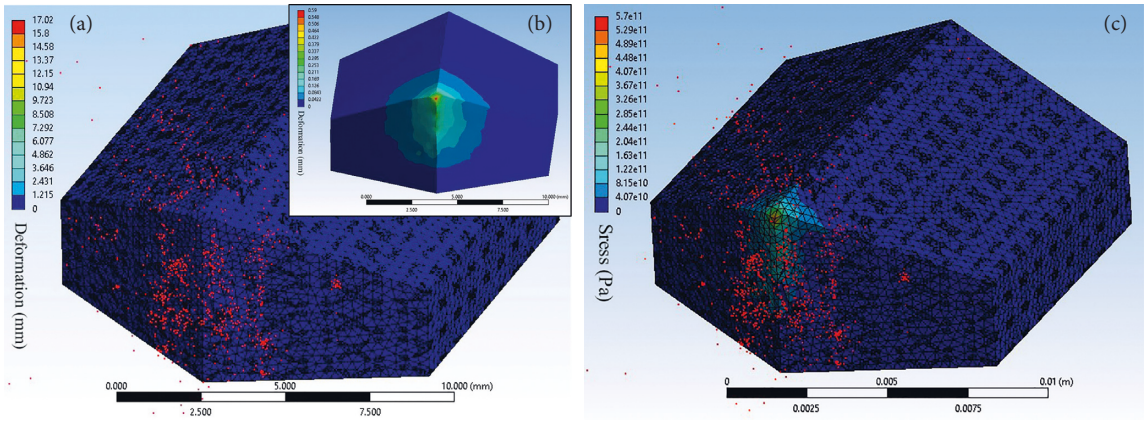

Figure 15: Deformation (a, b) and Von Mises stress distribution (c) of insert made of diamond with lattice. Red points of images (a) and (c) illustrate the fine particles of metal lattice that are relocated from the original position. Image B shows deformation of the material with excluded relocated particles.

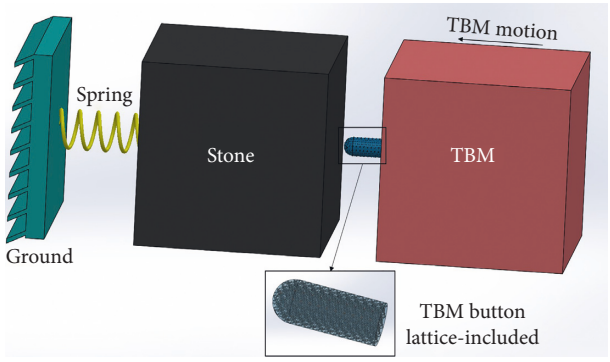

Figure 16: Schematic illustration of the modelling conditions of button impacting stone. The button and the stone are both modelled with inertia.

possible to the real ones. It was set that TBM button has a speed of 1 m/s while the stone was moving with a speed close to zero (0.1 mm/s). The results of deformation and Von Mises stress calculations for pure diamond and Ti6Al4V lattice-included diamond are shown in Figures 17 and 18, respectively. For pure diamond (Figure 17), deformation and stress concentration are located mainly in the tip area of a button and with a size of about 1 mm. The lattice-enhanced structure of diamond-based material transfers the deformation and stress concentration to the end of a button (Figure 18) where it is fixed to the TBM cutterhead (Figure 16) and consequently absorbs the impact intensity and increases the lifetime value of buttons. The performance of lattice during abrasion by insert and impact by button is illustrated in Figures 19(a) and 19(b), respectively. The results show that the whole lattice structure of the part is affected by abrasion or impact and helps to redistribute the stresses and increase the damage tolerance.

4. Conclusion

This study has described two novel approaches for reinforcement of the materials intended for improvement of performance in impact-abrasive conditions. Impact energy absorptive Ti6Al4V lattice along with diamond particles or

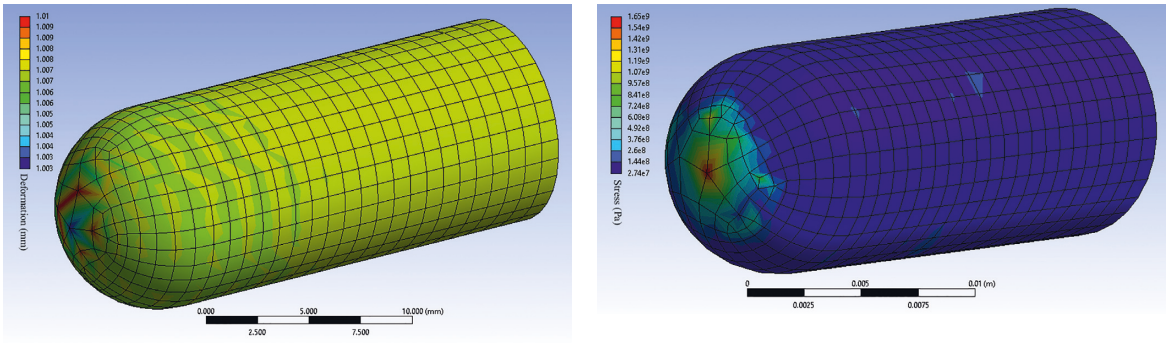

(a) (b)

Figure 17: Deformation (a) and Von Mises stress distribution (b) of solid diamond TBM button.

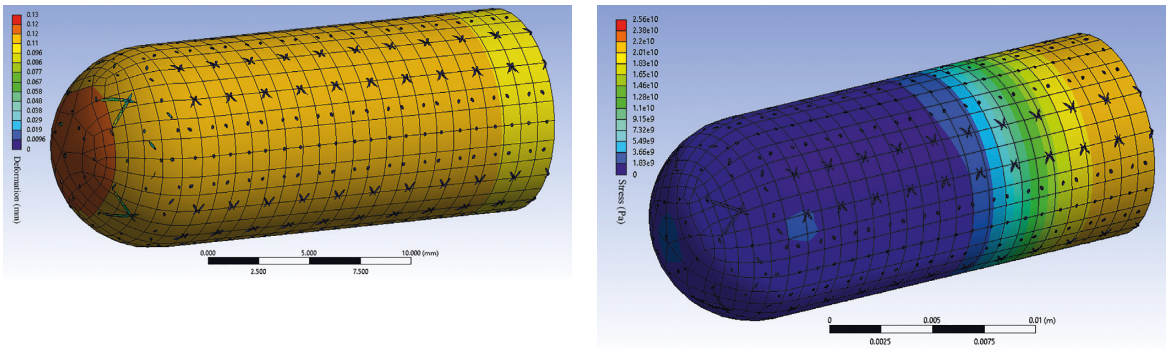

(a) (b)

Figure 18: Deformation (a) and Von Mises stress distribution (b) of button made of solid diamond with Ti6Al4V lattice.

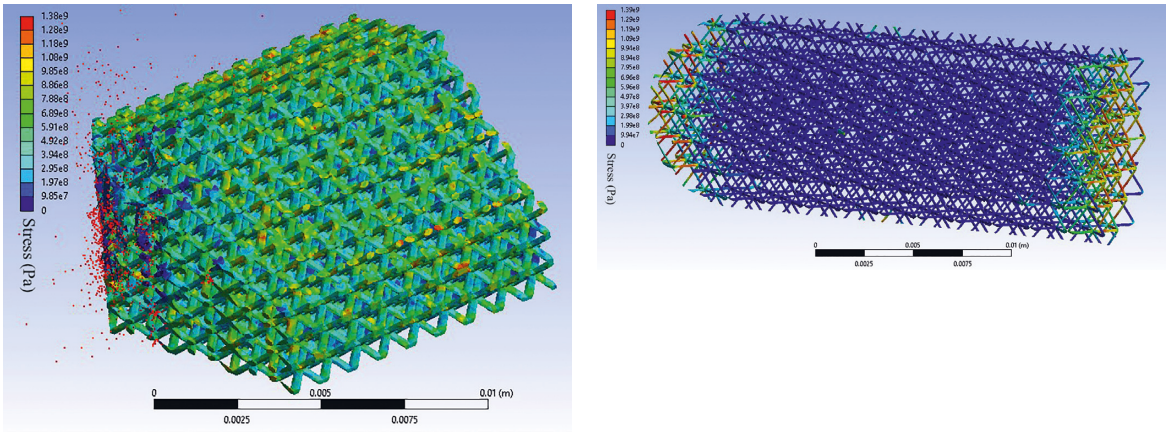

(a) (b)

Figure 19: Von Mises stress distribution of lattices shown separately for the conditions of abrasion (a) and impact (b).

nitrides improving wear resistance is introduced for the production of inserts and buttons of tunnelling machine:

(1) It was confirmed by laboratory testing that both approaches are providing up to 2.0 and 5.6 times improvement in wear resistance in impact-abrasive conditions. The reinforcement by diamond particles was providing the best improvement while reinforcement by nitriding of the lattice was less efficient. The lattice for both approaches was printed with the help of the SLM machine and later filled with powder and consolidated by applying the SPS method.

(2) It was shown that the combination of 3D printing of 316L-diamond lattice and SPS method has

provided uniform distribution of diamond particles. It was also found that the material with higher diamond content provides higher wear resistance.

(3) The use of diamond particles coated by nickel and fast-sintering time during SPS process helped to reduce graphitization of diamond that was confirmed by XRD and high performance of reinforced materials.

(4) The optimal nitriding conditions of 3D printed Ti6Al4V lattice structures (90 min at 900°C) and the unit cell size of the lattice (0.75 mm) were found.

(5) The modelling with the help of SOLIDWORKS/ANSYS finite element method proved that lattice structure enables to improve performance of materials in abrasive and impact conditions similar to those experienced by inserts and buttons of drag bit of soft ground TBM or those found in other applications (mining or geothermal drilling, for example).

Data Availability

The materials, techniques, machines, references, and simulation data used to support the findings of this study are included within the article.

Disclosure

The founding sponsors had no role in the design of the study; in the collection, analyses, or interpretation of data; in the writing of the manuscript, and in the decision to publish the results.

Conflicts of Interest

The authors declare that there are no conflicts of interest regarding the publication of this paper.

Authors' Contributions

Methodology, experiments, software analysis, writing, investigation, and visualization were carried out by R. R. Project administration, reviewing, editing, and supervision were performed by M. A. Printing assistance and supervision were carried out by L. K.

Acknowledgments

This research was supported by the Estonian Ministry of Education and Research (IUT 19–29 and ETAG18012); TALTECH base finance project (B56 and SS427); the personal grant of the Estonian Research Council (PUT1063); the European Regional Fund (2014-2020.4.01.16-0183) (Smart Industry Centre); and ASTRA "TALTECH Institutional Development Programme for 2016–2022" Graduate School of Functional Materials and Technologies (2014-2020.4.01.16-0032). The authors would like to thank Rainer Traksmaa for the help with preparation of XRD measurements.

References

[1] I. Yadroitsev and I. Smurov, "Selective laser melting technology: from the single laser melted track stability to 3D parts of complex shape," *Physics Procedia*, vol. 5, pp. 551–560, 2010.

[2] D. Dai and D. Gu, "Thermal behavior and densification mechanism during selective laser melting of copper matrix composites: simulation and experiments," *Materials and Design*, vol. 55, pp. 482–491, 2014.

[3] I. Yadroitsev, P. Krakhmalev, and I. Yadroitsava, "Selective laser melting of Ti6Al4V alloy for biomedical applications: temperature monitoring and microstructural evolution," *Journal of Alloys and Compounds*, vol. 583, pp. 404–409, 2014.

[4] Z. Sun, X. Tan, S. B. Tor, and W. Y. Yeong, "Selective laser melting of stainless steel 316L with low porosity and high build rates," *Materials and Design*, vol. 104, pp. 197–204, 2016.

[5] E. Brandl, U. Heckenberger, V. Holzinger, and D. Buchbinder, "Additive manufactured AlSi10Mg samples using Selective Laser Melting (SLM): microstructure, high cycle fatigue, and fracture behavior," *Materials and Design*, vol. 34, pp. 159–169, 2012.

[6] H. K. Rafi, N. V. Karthik, H. Gong, T. L. Starr, and B. E. Stucker, "Microstructures and mechanical properties of Ti6Al4V parts fabricated by selective laser melting and electron beam melting," *Journal of Materials Engineering and Performance*, vol. 22, no. 12, pp. 3872–3883, 2013.

[7] C. Yan, L. Hao, A. Hussein, and D. Raymont, "Evaluations of cellular lattice structures manufactured using selective laser melting," *International Journal of Machine Tools and Manufacture*, vol. 62, pp. 32–38, 2012.

[8] M. Smith, Z. Guan, and W. J. Cantwell, "Finite element modelling of the compressive response of lattice structures manufactured using the selective laser melting technique," *International Journal of Mechanical Sciences*, vol. 67, pp. 28–41, 2013.

[9] A. Hussein, L. Hao, C. Yan, R. Everson, and P. Young, "Advanced lattice support structures for metal additive manufacturing," *Journal of Materials Processing Technology*, vol. 213, no. 7, pp. 1019–1026, 2013.

[10] C. Yan, L. Hao, A. Hussein, P. Young, and D. Raymont, "Advanced lightweight 316L stainless steel cellular lattice structures fabricated via selective laser melting," *Materials and Design*, vol. 55, pp. 533–541, 2014.

[11] C. Yan, L. Hao, A. Hussein, S. L. Bubb, P. Young, and D. Raymont, "Evaluation of light-weight AlSi10Mg periodic cellular lattice structures fabricated via direct metal laser sintering," *Journal of Materials Processing Technology*, vol. 214, no. 4, pp. 856–864, 2014.

[12] V. J. Challis, X. Xu, L. C. Zhang, A. P. Roberts, J. F. Grotowski, and T. B. Sercombe, "High specific strength and stiffness structures produced using selective laser melting," *Materials and Design*, vol. 63, pp. 783–788, 2014.

[13] C. Qiu, S. Yue, N. J. E. Adkins et al., "Influence of processing conditions on strut structure and compressive properties of cellular lattice structures fabricated by selective laser melting," *Materials Science and Engineering: A*, vol. 628, pp. 188–197, 2015.

[14] C. Yan, L. Hao, A. Hussein, P. Young, J. Huang, and W. Zhu, "Microstructure and mechanical properties of aluminium alloy cellular lattice structures manufactured by direct metal laser sintering," *Materials Science and Engineering: A*, vol. 628, pp. 238–246, 2015.

[15] R. Wauthle, B. Vrancken, B. Beynaerts et al., "Effects of build orientation and heat treatment on the microstructure and mechanical properties of selective laser melted Ti6Al4V lattice structures," *Additive Manufacturing*, vol. 5, pp. 77–84, 2015.
[16] https://www.materials.sandvik/en/.
[17] http://www.tls-technik.de/.
[18] http://www.vanmoppes.ch/en/.
[19] http://www.nfm-technologies.com/.
[20] T. Camus and S. Moubarak, "Maintenance Robotics in TBM Tunnelling, ISARC," in *Proceedings of the International Symposium on Automation and Robotics in Construction*, Oulu, Finland, February 2015.
[21] M. Antonov, R. Veinthal, D.-L. Yung, D. Katušin, and I. Hussainova, "Mapping of impact-abrasive wear performance of WC-Co cemented carbides," *Wear*, vol. 332-333, pp. 971–978, 2015.
[22] R. Rahmani, M. Antonov, and L. Kollo, "Wear resistance of (diamond-Ni)-Ti6Al4V gradient materials prepared by combined selective laser melting and spark plasma sintering techniques," *Advances in Tribology*, vol. 2019, Article ID 5415897, 12 pages, 2019.
[23] Y. Holovenko, L. Kollo, M. Jõeleht, R. Ivanov, T. Soloviova, and R. Veinthal, "Production of metal-ceramic lattice structures by selective laser melting and carburizing or nitriding," *Proceedings of the Estonian Academy of Sciences*, vol. 68, no. 2, pp. 131–139, 2019.
[24] Y. Holovenko, M. Antonov, L. Kollo, and I. Hussainova, "Friction studies of metal surfaces with various 3D printed patterns tested in dry sliding conditions," *Proceedings of the Institution of Mechanical Engineers, Part J: Journal of Engineering Tribology*, vol. 232, no. 1, pp. 43–53, 2018.
[25] R. Rahmani, M. Antonov, and N. Kamboj, "Modelling of impact-abrasive wear of ceramic, metallic, and composite materials," *Proceedings of the Estonian Academy of Sciences*, vol. 68, no. 2, pp. 191–197, 2019.